Enhancement of dielectric and electro-optical characteristics of liquid crystalline material 4′-octyl-4-cyano-biphenyl with dispersed functionalized and nonfunctionalized multiwalled carbon nanotubes

Praveen Kumar Singh [1,*] Ravindra Dhar [1,†] and Roman Dabrowski [2]
[1]*Centre of Material Sciences, University of Allahabad, Prayagraj-211002, India*
[2]*Institute of Applied Sciences and Chemistry, Military University of Technology, Warsaw 00-908, Poland*

(Received 14 January 2023; accepted 1 March 2023; published 28 April 2023)

For recent applications, liquid crystal-carbon nanotube based nanocomposite systems have been proven to be highly attractive. In this paper, we give a thorough analysis of a nanocomposite system made of both functionalized and nonfunctionalized multiwalled carbon nanotubes that are disseminated in a 4′-octyl-4-cyano-biphenyl liquid crystal medium. Thermodynamic study reveals a decrease in the nanocomposites' transition temperatures. In contrast to nonfunctionalized multiwalled carbon nanotube dispersed systems, the enthalpy of functionalized multiwalled carbon nanotube dispersed systems has increased. In comparison to the pure sample, the dispersed nanocomposites have a smaller optical band gap. A rise in the longitudinal component of permittivity and, consequently, the dielectric anisotropy of the dispersed nanocomposites has been observed by dielectric studies. When compared to the pure sample, the conductivity of both dispersed nanocomposite materials has increased by two orders of magnitude. For the system with dispersed functionalized multiwalled carbon nanotubes, the threshold voltage, splay elastic constant, and rotational viscosity all decreased. For the dispersed nanocomposite of nonfunctionalized multiwalled carbon nanotubes, the value of the threshold voltage is somewhat decreased but the rotational viscosity and splay elastic constant both are enhanced. These findings show the applicability of the liquid crystal nanocomposites for display and electro-optical systems with appropriate tuning of the parameters.

DOI: 10.1103/PhysRevE.107.044704

I. INTRODUCTION

Carbon nanotubes (CNTs) have been employed for a wide range of applications due to their extraordinary characteristics and incredibly enormous surface area [1,2]. CNTs are hollow graphitic materials made of one or more layers of graphene sheets coaxially assembled [3]. The molecular and atomic properties of CNTs, which enable chemical stability, mechanical strength, electrical conductivity with ballistic transport behavior, and great flexibility, are what spark interest in them. CNTs offer a wide range of potential uses in a number of industrial fields, including nanocomposites for battery electrodes; in supercapacitors, energy storage, and conversion; nanoscale electronics; and liquid crystal (LC) display [1–5]. The alignment of the nanotubes is crucial for many of these applications. The alignment can be accomplished through applying external stimulation such as an electric or magnetic field, or mechanical stress to groups of synthesized tubes. However, research into employing these techniques to align nanotubes on a large scale is still in its early stages [6]. A fundamentally different concept that has recently been intensively investigated is dispersing CNTs in anisotropic organic matrices. Different self-assembling substances, including polymers, LCs, and surfactants, have been investigated as organic hosts for CNTs [7,8]. LCs are anisotropic material (having properties and symmetry associated with solid and liquids) in which some of the properties related with crystal and liquid coexists [9–11]. It has liquidlike fluidity and formation of droplets as well as solidlike anisotropy in optical, magnetic, and electrical properties [9–11]. LCs are characterized by a rigid core (mesogen) and aliphatic tail and show various phases called the mesophase which differ from each other due to different orientational order of individual molecules with different order in each phase. On the basis of their symmetry and structure LC phases are divided by their orientational and translational degrees of freedom. Nematic (*N*), smectic (Sm), and columnar (Col) phases possess three, two, and one translational degrees of freedom, respectively. In all of the above, nematic liquid crystal (NLCs) are the simplest, where molecules are oriented parallel to each other with zero or least positioning of molecules [9–14]. LCs appear as an exceptional material having a great impact on the development of liquid crystal displays (LCDs) [15–17]. A new era for the production of sophisticated materials in several domains of science and technology has begun as a result of the inclusion of various carbon nanostructures (CNSs) like CNTs into LCs [18–28]. LCs and CNTs have comparable forms of anisotropy, with LCs incorporating the tubes into their own structure. Due to improved intermolecular interaction, the combination of LCs with CNTs encourages varied physical features. The intermolecular interaction on the molecular level between LCs and CNTs leads the change in thermodynamic, electrical, and optical properties [29–33]. Strong π-π^* interactions between

*Corresponding author: praveenmsau@gmail.com
†Corresponding author: rdhar@allduniv.ac.in

LCs and tubes have improved the dielectric and electro-optical responsiveness [34–37]. Chemical functionalization of tubes has become a hot topic in recent study using CNTs as a basic material. Functionalization typically results in the breaking of tube bundles, increasing molecule polarizability and dipole moment, and enhancing the intermolecular interaction with LCs [38,39]. Various studies have been carried out to enhance the physical and rheological properties of original LCs by dispersion of functionalized CNTs [40,41]. Kumar *et al.* have reported a change in electro-optical properties of LCs dispersed with functionalized single-walled carbon nanotubes (FSWCNTs) [42].

Here we present the dispersion of 0.5 wt % of nonfunctionalized and functionalized multiwalled carbon nanotubes (NFMWCNTs and FMWCNTs) in the LC host 4′-octyl-4-cyano-biphenyl (8CB). Various studies on 8CB have been reported [43,44]. We demonstrate the effect on thermodynamic, optical, dielectric, and electro-optical properties of the LC host dispersed with NFMWCNTs and FMWCNTs. Comparative study of different concentrations has been done. In recent publication, 0.05 wt % of NFMWCNTs and FMWCNTs was dispersed in the same host of 8CB [45]. The NFMWCNTs (purity: >95%, outer diameter: 8–15 nm) used in this work is purchased from Time Nano, China. Chemical functionalization, preparation of the nanocomposite, and characterization have been done as reported in our earlier publication [45].

II. MEASUREMENT TECHNIQUES

A differential scanning calorimeter (DSC) (model DSC-200-F3 Maia, Netzsch, Germany) was used to determine the transition temperature, enthalpy, and entropy of the materials studied here [46]. The instrument was properly calibrated by using spec pure indium and zinc as standard calibrants. Initially, five thermal cycles of heating and cooling were done at the scan rate of 15 °C/ min in order to stabilize the samples. Thereafter, samples were scanned at different rates between 2.5 °C/ min and 12.5 °C/min to record the variations of transition temeratures with the scanning rate. For the thermodynamic study, small amounts of the samples (2–5 mg) were kept in the sample holder and DSC thermograms at various scanning rates were recorded. With these thermograms, transition temperatures were determined with an accuracy of ±0.1 °C whereas transition enthalpy measurements have a margin of error in the range of 2%–5%. A polarized optical microscope (POM) (model 108329, CENSICO, India) was used to record optical textures. The transmission intensity of white light has been measured by using a photodetector (model PD-02, Instec, USA) connected with the POM. An impedance analyzer (model Alpha-A high-frequency impedance analyzer, Novocontrol Technologies, Germany) was used to conduct dielectric tests in the frequency range of 1 Hz–40 MHz. A measuring voltage of 0.5 V_{rms} was applied across the samples. Dielectric cells in the form of parallel plate capacitors were prepararred with indium tin oxide (ITO) coated glass plates (sheet resistance ∼ 25 Ω/□) as electrodes. Separation between the electrodes was maintained by mylar spacers of thickness 10 μm. Appropriate chemical coatings on the ITO coated surfaces were made to obtain planar and homeotropic alignments of the liquid crystal molecules. These cells were used for both dielectric and electro-optical experiments. Error in the measurements of dielectric parameters is less than 2%. The electro-optical study was done with the help of a photodetector which is mounted on the POM. Measurement of photovoltage was performed with a six and a half digit multimeter (model 34410A, Agilent, USA). Further experimental details can be seen in our earlier work [45,47,48].

III. RESULTS AND DISCUSSION

Thermodynamic, optical, dielectric, and electro-optical results obtained on 8CB and its nanocomposites with NFMWCNTs and FMWCNTs are discussed in the following subsections.

A. Thermodynamic study

DSC has been used to accomplish thermodynamic studies on the materials in pure 8CB as well as its nanocomposites. Figure 1 displays the variation of heat flow with temperature at a scan rate of 2.5 °C/ min. Thermodynamic investigation shows that, in comparison to pure 8CB LCs, the transition temperatures from Cry to Sm*A* phase, Sm*A* to *N* phase, and *N* to *I* phase decrease with the dispersion of both FMWCNTs and NFMWCNTs for both heating and cooling cycles. In a recent publication the transition temperature was increased due to mutual alignment of tubes with the director of the LCs [45]. At lower concentration the anisotropy of the nanocomposite system is not changed as compared to the pure sample by which LCs and CNTs are aligned along a long molecular axis. The enthalpy and entropy of the nanocomposite were increased due to mutual alignment of the tubes and the LC molecule. Enhanced order parameters were found for the nanocomposite system [45]. In the present study, due to strong anchoring between the LCs and CNTs, the development of a honeycomb lattice, the existence of hydrogen bonds, and formation of aggregates, as well as the dilution effect, are all likely to be contributing factors to the decrease in transition temperature [49,50]. At higher concentration the anisotropy of the host is different than the nanocomposite system due to a difference in the dipole moment. At this concentration there are some aggregate forms which decrease the order parameters and hence the enthalpy of the nanocomposite system. Due to the potent π-π^* interactions of aromatic cores with the honeycomblike arrangement of the CNT walls, the nanotubes are distributed along the *N* director. It should be noted that these aromatic cores contain LC molecules with phenyl rings. The hydrogen bonding between the 8CB LC cyano group and the -COOH functionalization group of CNT also caused the *N*-*I* phase transition temperatures in FMWCNTs to decrease more in comparison to NFMWCNTs. Due to the -COOH group's linkage, the obstruction in FMWCNTs that was brought on by carbon-to-carbon aggregation in the tubes has been reduced. By increasing the distance between carbon atoms, which were previously plain (smooth) in the case of NFMWCNTs, the surface is deformed. The reactive surface area of the tubes has grown, increasing the anchoring energy and resulting in improved tube dispersion in LC me-

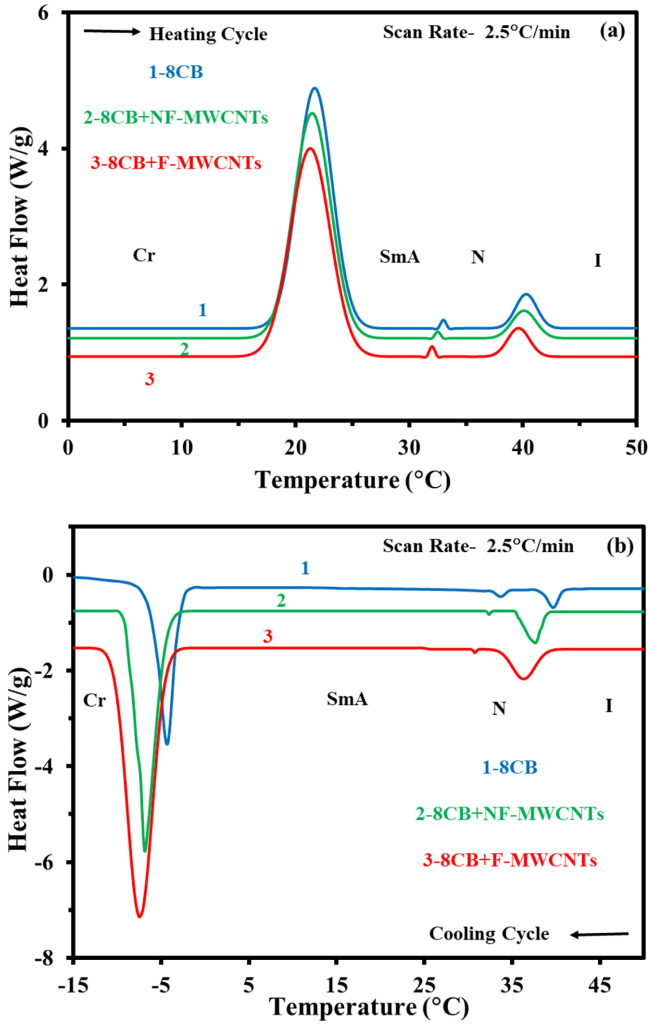

FIG. 1. DSC thermograms of the pure and dispersed samples at a scan rate of 2.5 °C/min during (a) heating, (b) cooling cycle. Curves 1–3 are for the pure 8CB, 8CB+NFMWCNTs, and 8CB+FMWCNTs, respectively.

dia. As a result, FMWCNTs cause LCs' molecular structure to alter more, which lowers the transition temperature [51]. According to Chen *et al.* FMWCNTs have an impact on morphology and transition temperatures because they reduce the viscosity of the nanocomposite, which functions as a supercooled liquid [52]. Table I displays the values of the thermodynamic parameters. We deduced from the DSC curve that the FMWCNTs' dispersed sample has a higher value of change in enthalpy for Sm*A*-*N* and *N*-*I* transitions than the NFMWCNTs dispersed sample does. When FMWCNTs are disseminated in a nanocomposite, the width of the transition peak decreases, whereas when NFMWCNTs are dispersed in a nanocomposite, it increases. The height of the transition peak is decreased in the nanocomposite system dispersed with NFMWCNTs, whereas the height of the transition peaks is elevated for the FMWCNTs dispersed nanocomposite. The creation of aggregation, which reduces the order parameters of the NFMWCNTs dispersed nanocomposite, is the sole cause of the drop in enthalpy, rise in width, and suppression of the peak's height. Due to the improvement of the order parameters, the dispersed nanocomposite of FMWCNTs exhibits the opposite trend.

B. Texture study

The POM is a useful tool for determining the LC phases and phase transition temperatures. Optical textures of the unaligned samples under the cover slips (shown in Fig. 2) were recorded during the cooling cycles to confirm various phases and transition temperatures obtained by DSC. Schlieren texture appeared for the *N* phase while fan shaped texture appeared in the Sm*A* phase for pure and dispersed samples. However, optical textures of unaligned samples did not show any clear signature of MWCNTs in the LC medium due to the defects present in the unaligned samples. Therefore, in order to verify the uniform dispersion of MWCNTs in the LC matrix, homogeneous textures of pure 8CB and its nanocomposite were recorded in planar aligned samples and shown in Fig. 3. Figure 3(b) shows that the disseminated NFMWCNTs nanocomposite forms some aggregates, which vanish when the same concentration of FMWCNTs was dispersed [see Fig. 3(c)] in the host of LC molecules. Thus, functionalization has been instrumental for the uniform distribution of MWCNTs in a LC matrix. The phase sequence and transition temperatures obtained by DSC study matched with those obtained by POM when compared for the same (slowest) scan rate.

C. Ultraviolet-visible (UV-vis) study

The UV-vis absorption spectra of pure 8CB, NFMWCNTs, and FMWCNTs dispersed nanocomposites dissolved in cyclohexane were measured at wavelengths between 220 and 520 nm [53]. The absorption peak appears at 316.0, 284.5, and 282.5 nm for 8CB, NFMWCNTs, and FMWCNTs dispersed nanocomposites, respectively, as shown in Fig. 4. The optical band gaps (E_g) have been determined (see Fig. 5) using the Tauc equation as

$$\alpha h\nu = (h\nu - E_g)^{1/q}, \tag{1}$$

where $h\nu$ is the incident photon energy, α is the absorption coefficient, and q characterizes the nature of the transition [47]. E_g has been estimated as 3.95, 3.68, and 3.79 eV for pure 8CB, NFMWCNTs, and FMWCNTs dispersed nanocomposites, respectively, from Fig. 5. The result shows a decline in E_g for dispersed nanocomposites. E_g has decreased as a result of the NFMWCNTs' and FMWCNTs' conductivity. In a recent publication, the value of E_g is 3.63 eV, and 3.83 eV for NFMWCNTs and FMWCNTs dispersed nanocomposites for the concentration of 0.05 wt % [45]. At higher concentration due to the formation of some aggregates the value of E_g is increased marginally for NFMWCNTs dispersed nanocomposite whereas due to higher dispersibility of FMWCNTs the value of E_g is decreased marginally as observed in Fig. 5. The delocalized electrons in NFMWCNTs and FMWCNTs dispersed nanocomposites absorb the photon rather easily due to a smooth charge transfer mechanism between LCs and CNTs. The value of E_g is also shown in Table II.

TABLE I. Thermodynamic parameters of 8CB, 8CB+NFMWCNTs, and 8CB+FMWCNTs at a scan rate of 2.5 °C/min.

Material	Transition Temperature (T_p) (°C)	Enthalpy (ΔH, J/g)	Width (°C)	Height (J/g s)	Entropy (ΔS, J/g K)
Heating cycle					
Cry-Sm*A*					
8CB	24.2	79.5	3.41	3.30	0.25
8CB+NFMWCNTs	20.5	71.3	3.82	2.87	0.24
8CB+FMWCNTs	18.2	75.6	3.76	2.86	0.26
Sm*A*-*N*					
8CB	33.8	0.27	0.90	0.17	0.001
8CB+NFMWCNTs	30.8	0.25	0.92	0.16	0.002
8CB+FMWCNTs	30.0	0.28	0.88	0.18	0.001
N-*I*					
8CB	40.5	1.77	1.27	0.34	0.006
8CB+NFMWCNTs	39.4	1.73	1.33	0.30	0.005
8CB+FMWCNTs	38.4	1.89	1.24	0.38	0.008
Cooling cycle					
I-*N*					
8CB	40.3	1.91	1.31	0.37	0.006
8CB+NFMWCNTs	38.2	1.86	1.38	0.32	0.005
8CB+FMWCNTs	38.1	1.98	1.28	0.38	0.008
N-Sm*A*					
8CB	33.6	0.23	0.48	0.18	0.0007
8CB+NFMWCNTs	30.6	0.22	0.52	0.16	0.001
8CB+FMWCNTs	15.5	0.77	0.64	0.51	0.002
Sm*A*-Cry					
8CB	−3.57	75.8	2.28	2.90	0.28
8CB+NFMWCNTs	−3.70	73.5	2.34	3.30	0.27
8CB+FMWCNTs	−9.90	72.4	2.30	3.10	0.27

D. Dielectric studies

A dielectric study has been done in the frequency range of 1 Hz–40 MHz. The frequency range 100 Hz–100 kHz corresponds to bulk polarization and the charge transfer mechanism [54–57]. The dielectric property depends upon the structural arrangement of atoms/molecules and molecular polarizability. Hence, probing dielectric properties, gives indication of structural modification of the LC system in the presence of CNTs.

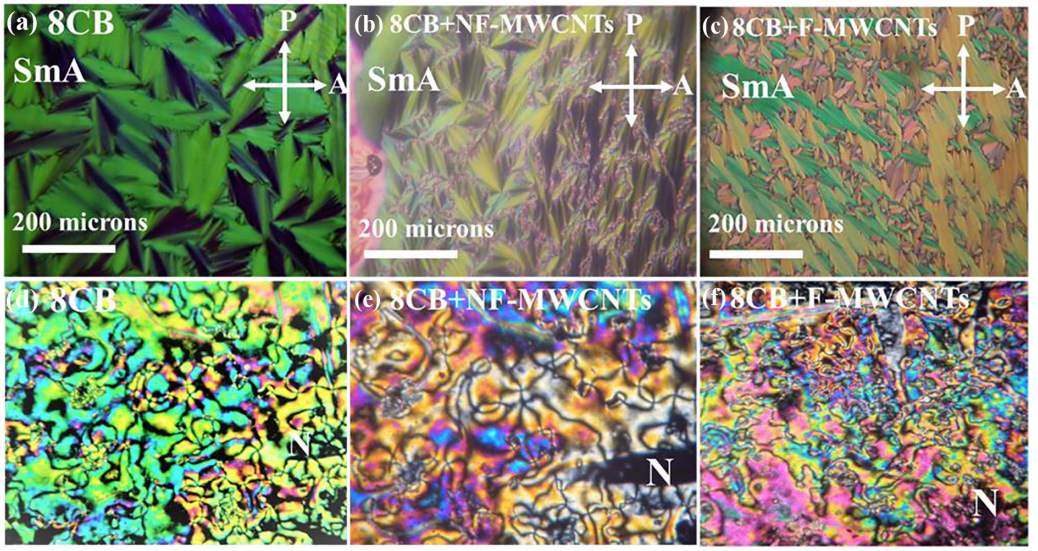

FIG. 2. Optical textures of (a) 8CB, (b) 8CB+NFMWCNTs, and (c) 8CB+FMWCNTs in the smectic *A* phase and (d) 8CB, (e) 8CB+NFMWCNTs, and (f) 8CB+FMWCNTs in the nematic phase under the cover slips.

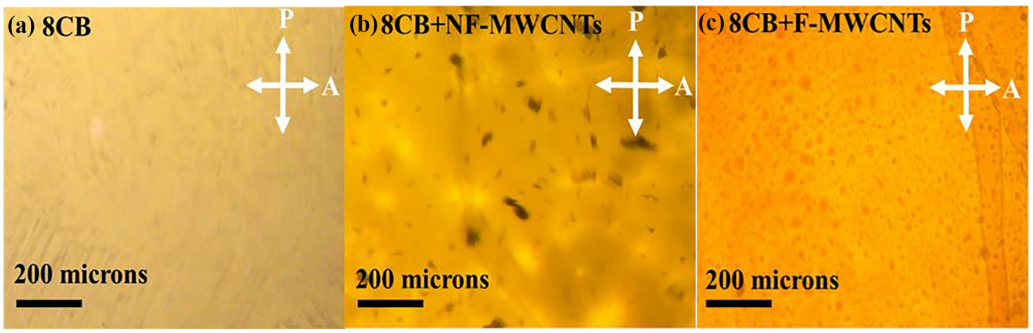

FIG. 3. Optical textures of (a) 8CB, (b) 8CB+NFMWCNTs, and (c) 8CB+FMWCNTs in the nematic phase just below the *I*-*N* transition during the cooling cycle for the homogeneously aligned molecules.

The dielectric spectra were fitted to the generalized Cole-Cole equation to calculate the relaxation frequency (f_r) and other dielectric parameters. The generalized Cole-Cole equation for the complex permittivity (ε^*) is given as [57,58]

$$\varepsilon^* = \varepsilon' - j\varepsilon'' = \varepsilon'(\infty) + \frac{\delta\varepsilon}{1+(j\tau f)^{(1-\alpha)}} + \frac{A}{f^m} - j\frac{\sigma_d}{\varepsilon_0 f^l} - jBf^n. \quad (2)$$

The above equation can be further separated into real, i.e., permittivity (ε'), and imaginary, i.e., loss (ε'') parts of the ε^* in the following way:

$$\varepsilon' = \varepsilon'(\infty) + \frac{\delta\varepsilon[1+(\tau f)^{(1-\alpha)}\sin(\alpha\pi/2)]}{1+(\tau f)^{2(1-\alpha)}+2(\tau f)^{(1-\alpha)}\sin(\alpha\pi/2)} + \frac{A}{f^m}, \quad (3)$$

$$\varepsilon'' = \frac{\delta\varepsilon(\tau f)^{(1-\alpha)}\cos(\alpha\pi/2)}{1+(\tau f)^{2(1-\alpha)}+2(\tau f)^{(1-\alpha)}\sin(\alpha\pi/2)} + \frac{\sigma_d}{\varepsilon_0 f^l} + Bf^n, \quad (4)$$

where $\delta\varepsilon = \varepsilon(0) - \varepsilon(\infty)$ is the dielectric strength of relaxation mode with $\varepsilon(0)$ and $\varepsilon(\infty)$ as the low- and high-frequency limiting values of ε'. ε_o is the free space permittivity. The distribution parameter α has a value in the range $0 < \alpha < 1$. $\tau(= 1/f_r)$ is the relaxation time. A and B are constants. The role of the electrode polarization capacitance and dc conductivity (σ_d) at lower frequencies [54,56] is represented by the third and fourth terms in the r.h.s of Eq. (2). The fifth imaginary term Bf^n is included in Eq. (2) to partially account for the sheet resistance of ITO coated glass plates and lead inductance used to fabricate cells [57]. The measured ε' and ε'' are separately fitted with Eqs. (3) and (4). Thus, the low- and high-frequency correction terms along with different parameters are obtained by the best fitting of these equations to the experimental data.

Due to the molecular rotation about their short axis, a relaxation phenomenon has been seen in the MHz region for the homeotropic alignment of the molecules. Figure 6 (for 8CB), Fig. 7 (for 8CB+NFMWCNTs nanocomposite), and Fig. 8 (for 8CB+FMWCNTs nanocomposite) depict the frequency dependence of the longitudinal component of the permittivity ($\varepsilon'_{||}$) and loss ($\varepsilon''_{||}$) for the Sm*A* (24.0 °C), as well as *N* (34.0 °C) phases. The Cole-Cole equation is used to fit the measured values of ε' and ε'' in order to eliminate the parasitic effect that occurs at low- and higher-frequency regions. By using the Cole-Cole equation, f_r has been determined. In

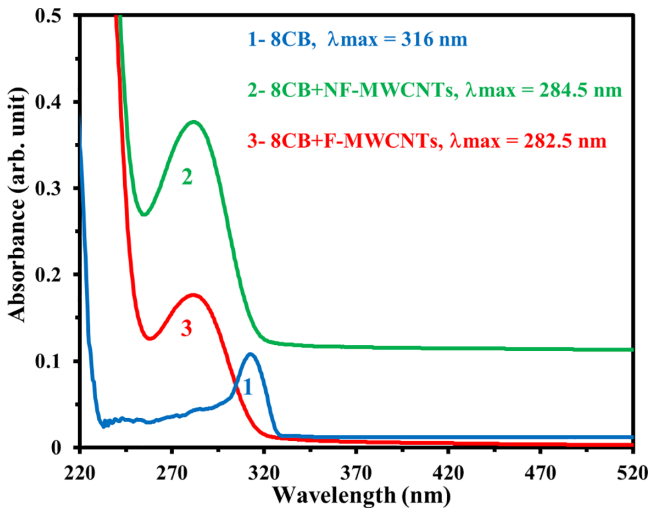

FIG. 4. UV-visible absorption spectra of (1) pure 8CB, (2) 8CB+NFMWCNTs, and (3) 8CB+FMWCNTs.

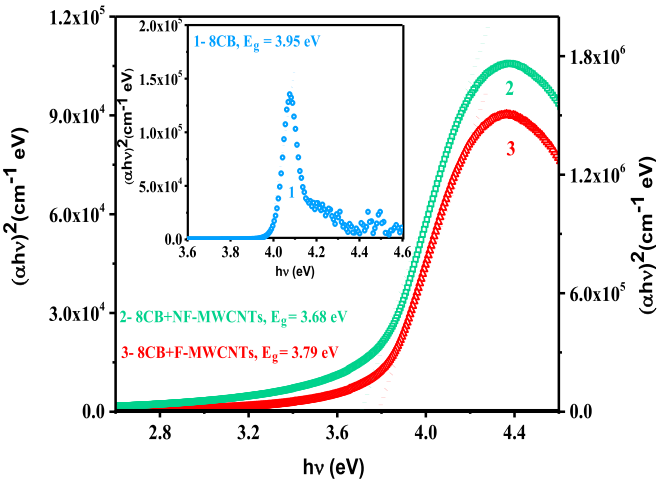

FIG. 5. Determination of the optical band gap (E_g) for (1) 8CB (inset), (2) 8CB+NFMWCNTs (l.h.s. scale), and (3) 8CB+FMWCNTs (r.h.s. scale).

TABLE II. Determination of the optical band gap of 8CB, NFMWCNTs, FMWCNTs, 8CB+NFMWCNTs, and 8CB+FMWCNTs.

Material	Optical band gap E_g (eV)
8CB	3.95
NFMWCNTs	3.84
FMWCNTs	4.15
8CB+NFMWCNTs	3.68
8CB+FMWCNTs	3.79

the Sm*A* phase f_r is 3.1 MHz for 8CB, and 2.8 MHz for NFMWCNTs dispersed nanocomposite, while it is 2.3 MHz for FMWCNTs dispersed nanocomposite. In the *N* phase f_r is 4.9 MHz for 8CB, 5.2 MHz for NFMWCNTs, and 7.1 MHz for FMWCNTs dispersed nanocomposite. Figure 9 (for 8CB), Fig. 10 (for 8CB+NFMWCNTs nanocomposite), and Fig. 11 (for 8CB+FMWCNTs nanocomposite) show plots of

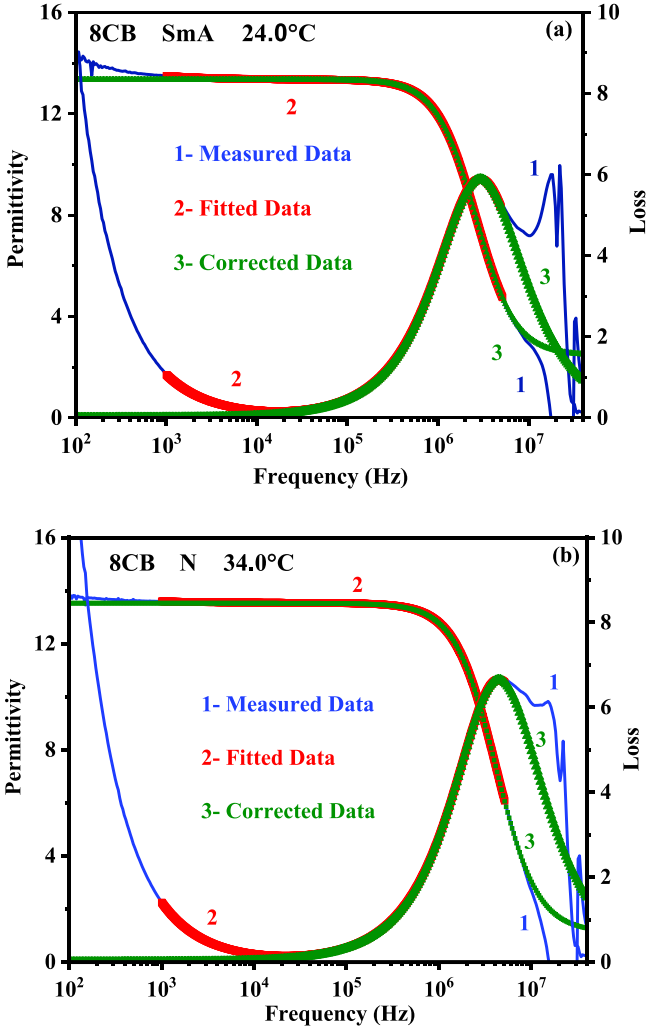

FIG. 6. Frequency dependence of the longitudinal component of the permittivity ($\varepsilon_{||}^{'}$) and loss ($\varepsilon_{||}^{''}$) for pure 8CB in (a) Sm*A* and in (b) *N* phase. Here 1–3 represent the measured, fitted, and corrected data for the permittivity and loss, respectively.

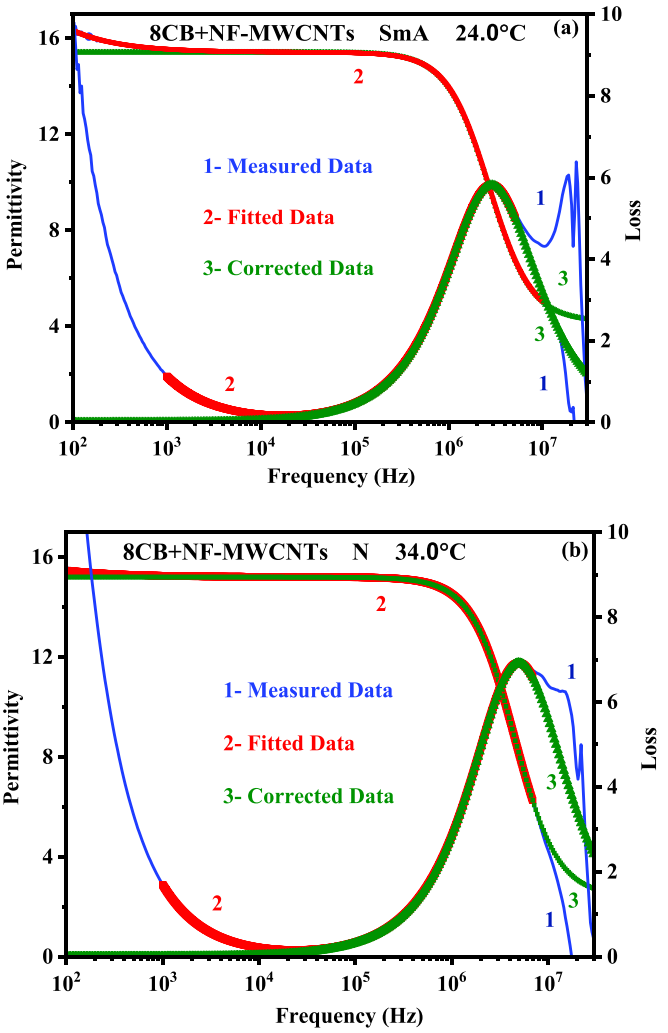

FIG. 7. Frequency dependence of the longitudinal component of the permittivity ($\varepsilon_{||}^{'}$) and loss ($\varepsilon_{||}^{''}$) for 8CB+NFMWCNTs in (a) Sm*A* and in (b) *N* phase. Here 1–3 represent the measured, fitted, and corrected data for the permittivity and loss, respectively.

$\varepsilon_{||}^{''}$ with $\varepsilon_{||}^{'}$ that resemble a semicircle and favor the relaxation phenomenon like the Debye process.

The temperature dependence of dielectric anisotropy ($\Delta\varepsilon^{'} = \varepsilon_{||}^{'} - \varepsilon_{\perp}^{'}$) has been plotted for pure as well as both dispersed samples as shown in Fig. 12. $\Delta\varepsilon^{'}$ for the *N* phase has been calculated for pure 8CB, NFMWCNTs dispersed, and FMWCNTs dispersed nanocomposite. The value of $\Delta\varepsilon^{'}$ is 7.1, 9.0, and 11.0 for pure 8CB, NFMWCNTs, and FMWCNTs dispersed nanocomposite, respectively. In the Sm*A* phase, it is 7.7, 10.1, and 12.5 for pure 8CB, NFMWCNTs, and FMWCNTs dispersed nanocomposite. In a recent publication [45] the value of $\Delta\varepsilon^{'}$ is 9.5 and 10.5 in the Sm*A* and *N* phase, respectively, for NFMWCNTs dispersed nanocomposite, while for FMWCNTs dispersed nanocomposite it is 10.5 and 12.1 in the Sm*A* and *N* phase, respectively. The value of $\Delta\varepsilon^{'}$ is decreased for NFMWCNTs dispersed nanocomposite as compared to the lower concentration and it is increased for the FMWCNTs dispersed nanocomposite as compared to the lower concentration reported earlier [45]. Due to a decrease of the order

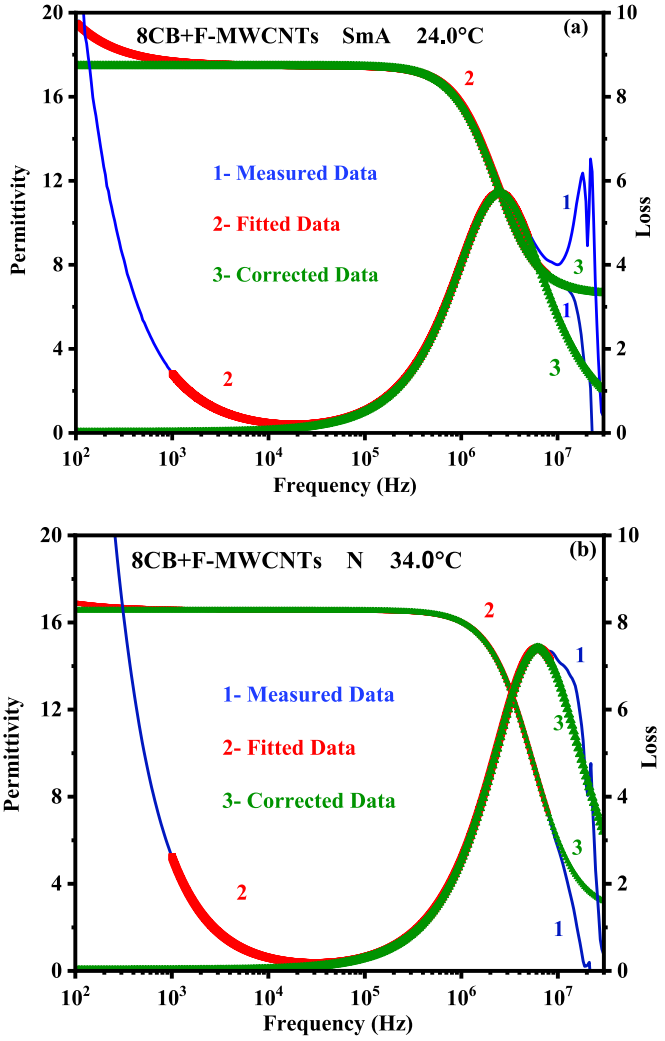

FIG. 8. Frequency dependence of the longitudinal component of the permittivity ($\varepsilon_{||}^{'}$) and loss ($\varepsilon_{||}^{''}$) for 8CB+FMWCNTs in the (a) Sm*A* and (b) *N* phase. Here 1–3 represent the measured, fitted, and corrected data for the permittivity and loss, respectively.

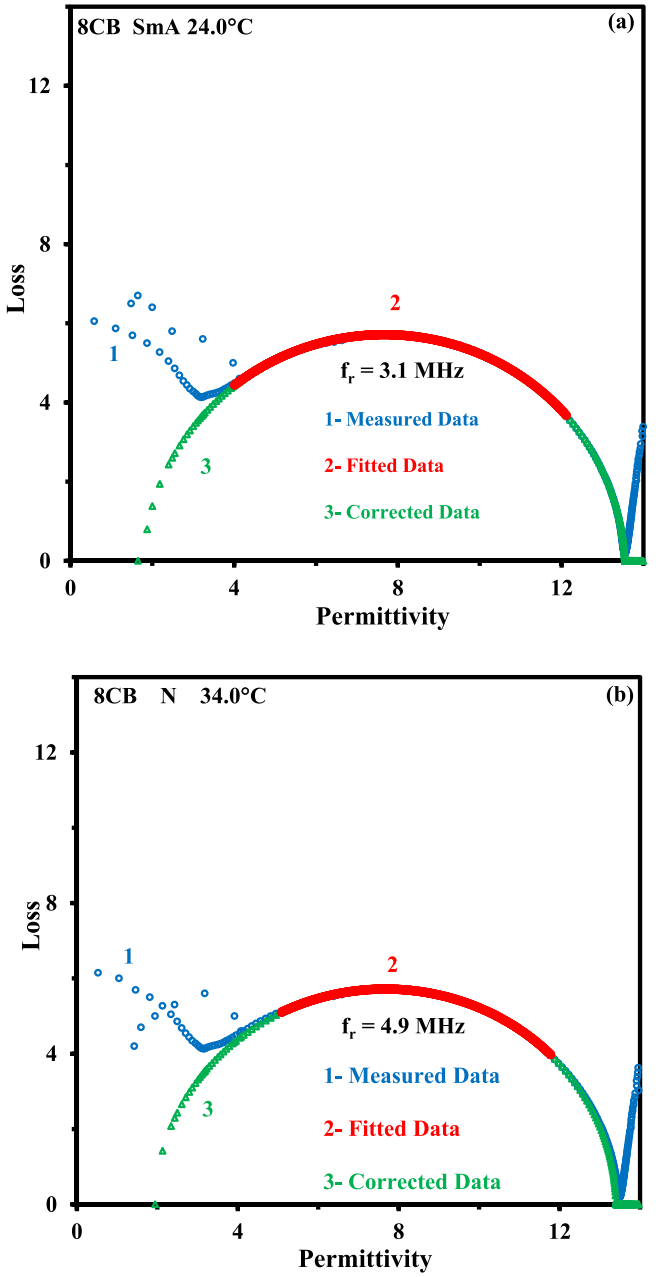

FIG. 9. Cole-Cole plots showing the variation of loss ($\varepsilon_{||}^{''}$) with permittivity ($\varepsilon_{||}^{'}$) for pure 8CB in (a) Sm*A* phase and in (b) *N* phase, respectively.

parameters the value of $\Delta\varepsilon^{'}$ is decreased for the NFMWCNTs dispersed nanocomposite while with the enhanced order parameters for the FMWCNTs dispersed nanocomposite the value of $\Delta\varepsilon^{'}$ is increased. A higher value of $\Delta\varepsilon^{'}$ is favored by the dipolar orientation of the LC molecules in the presence of the tubes. It is also noticed that the high anchoring energy produced by the tubes is also responsible for the increment in $\Delta\varepsilon^{'}$. The reason why the FMWCNTs dispersed nanocomposite has a greater value of $\Delta\varepsilon^{'}$ than NFMWCNTs dispersed nanocomposite is because the functional group connected to the MWCNTs has a higher dipole moment and polarizability. The longitudinal component of ε' is directly affected by dimerization and also due to enhanced aromatic character [59]. Various dielectric parameters are shown in Table III.

Temperature dependence of the relaxation phenomenon for the homeotropic aligned molecules has been observed for pure and MWCNT dispersed nanocomposites. The f_r increases with temperature following the Arrhenius behavior as

$$\log(f_r) = \log(f_0) - \frac{W_a}{RT}, \tag{5}$$

where R is the gas constant and T is the absolute temperature. The variation of f_r with the inverse of temperature is shown for both the Sm*A* and *N* phases in Fig. 13. With the help of the slope of a straight line found by the least-squares fit, the activation energy (W_a) has been calculated. W_a is 23.7 kJ mol^{-1} and 74.3 kJ mol^{-1} in Sm*A* and *N* phase respectively for pure 8CB. For NF-MWCNTs and F-MWCNTs dispersed nanocomposite W_a is 38.5 kJ mol^{-1} and 49.7 kJ mol^{-1} in the Sm*A* phase while it is 82.7 kJ mol^{-1} and 93.5 kJ mol^{-1} in the

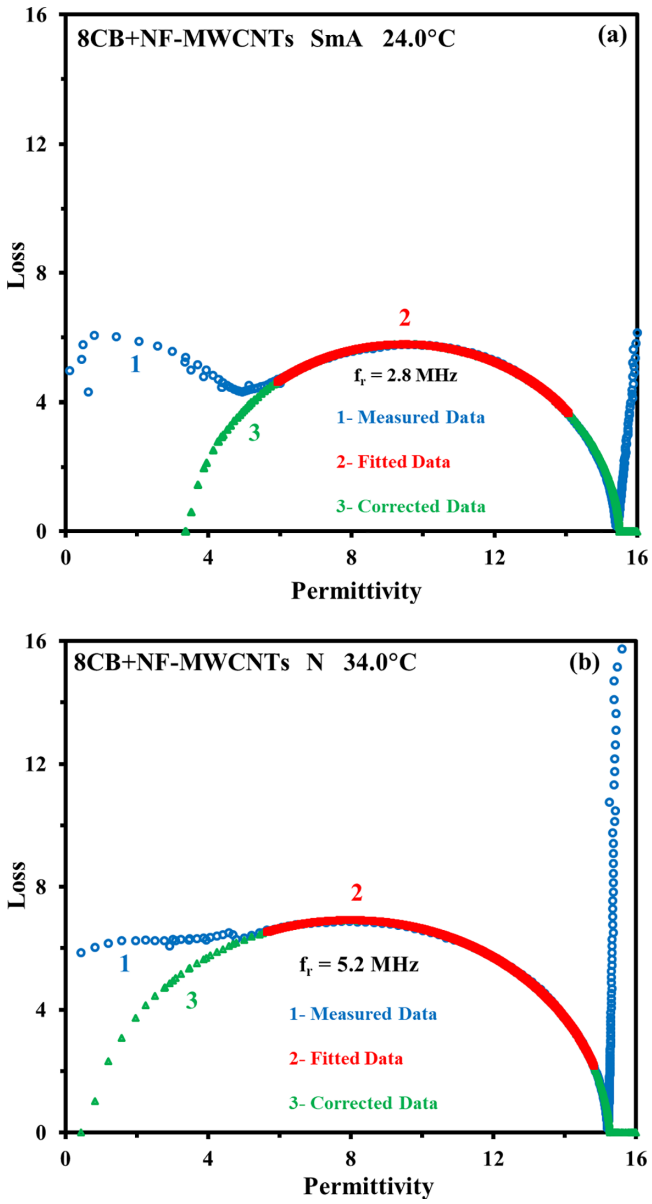

FIG. 10. Cole-Cole plots showing the variation of loss ($\varepsilon''_{||}$) with permittivity ($\varepsilon'_{||}$) for 8CB+NFMWCNTs in (a) Sm*A* phase and in (b) *N* phase.

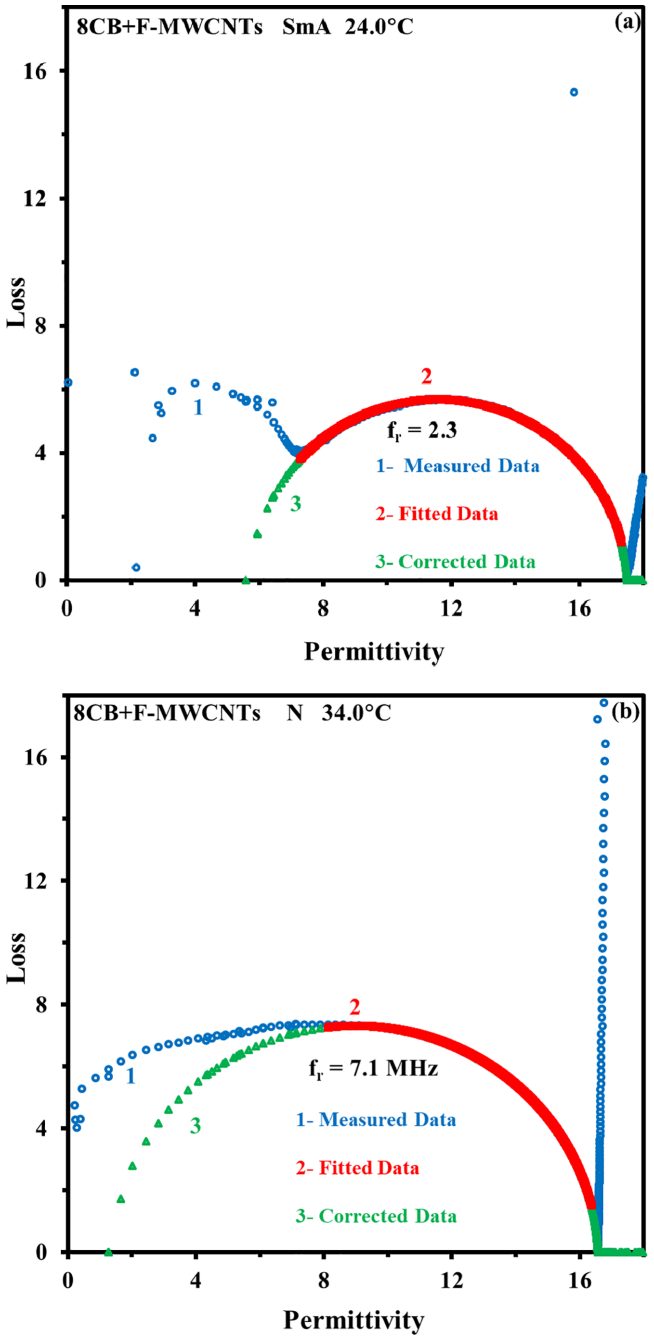

FIG. 11. Cole-Cole plots showing the variation of loss ($\varepsilon''_{||}$) with permittivity ($\varepsilon'_{||}$) for 8CB+FMWCNTs in (a) Sm*A* phase and in (b) *N* phase.

N phase. The higher value of W_a for FMWCNTs dispersed nanocomposite corresponds to the higher anchoring energy produced at the surface of the nanotubes which orient the LC molecule along their long axes easily.

Electrical conductivity is based on the characteristics of the charge carriers' conduction process and how they respond to frequency and temperature. The frequency dependence of the total conductivity (σ) generally follows Jonscher's power law [60] given as

$$\sigma(f) = \sigma_d + Cf^z. \tag{6}$$

σ_d is frequency independent dc conductivity; Cf^z is ac conductivity having characteristics of the power law in terms of frequency f and exponent z. The interaction between mobile ions and the lattice surrounding them is represented by exponent z. The strength of polarizability is demonstrated by constant C. At low frequencies (<1–10 kHz), the Cf^z term in Eq. (6) is minimal, and the only conductivity present is σ_d [61]. Frequency dependence of the conductivity is shown in Fig. 14 for pure 8CB and dispersed systems. From the graph it is clear that σ for NFMWCNTs and FMWCNTs dispersed nanocomposites has increased as compared to that of the pure sample. The excess delocalized π electron in NFMWCNTs and FMWCNTs gives a higher value of σ. In a recent publication (0.05 wt % NFMWCNTs and FMWCNTs in 8CB) the σ of NFMWCNTs dispersed nanocomposite was increased two

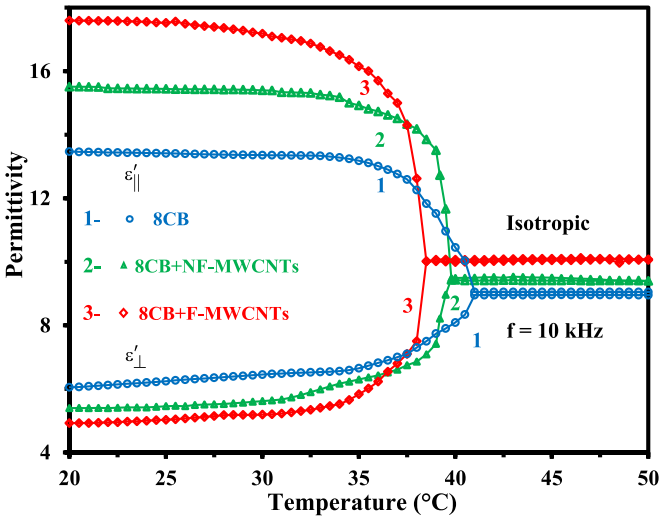

FIG. 12. Temperature dependence of the longitudinal ($\varepsilon'_{||}$) and transverse ($\varepsilon'_{\perp}$) components of the permittivity at 10 kHz of the frequency for (1) 8CB, (2) 8CB+NFMWCNTs, and (3) 8CB+FMWCNTs.

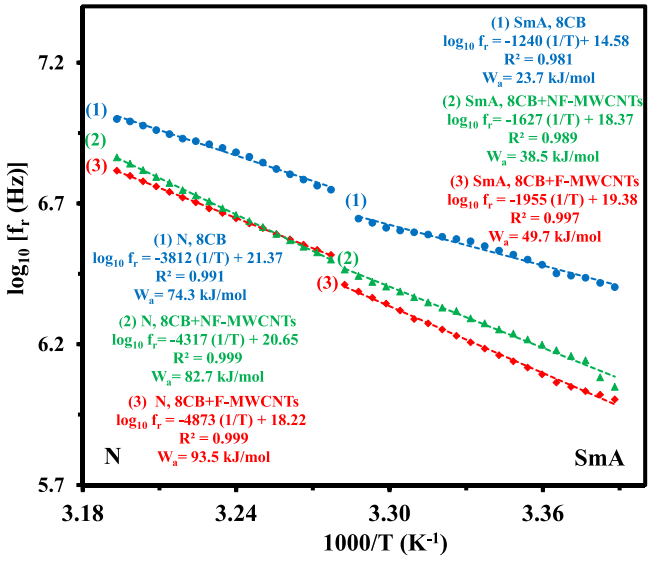

FIG. 13. Variation of the $\log_{10}$ of the relaxation frequency (f_r) with the inverse of the absolute temperature (K^{-1}) for (1) 8CB, (2) 8CB+NFMWCNTs, and (3) 8CB+FMWCNTs in Sm*A* and in *N* phases, respectively.

orders of magnitute as compared to the pure sample whereas it was the same as the pure sample for FMWCNTs dispersed nanocomposite [45]. In this work as the concentration is increased the σ of the NFMWCNTs dispersed nanocomposite is not altered as compared to the previously reported data [45], but it has increased for the FMWCNTs dispersed nanocomposite. Formation of some aggregates for this concentration of NFMWCNTs is the reason why the conductivity has not increased.

Figure 15 shows the dependence of the σ_d (determined by taking average of the constant region of Fig. 14) with temperature. The activation energy (E_a) for the σ_d is calculated from the Arrhenius equation given as

$$\sigma_d = D \exp(-E_a/k_B T), \tag{7}$$

where D is the preexponential factor and k_B is the Boltzmann constant. The slopes of the plots of $\log \sigma_d$ versus the inverse of the temperature were obtained by the method of least-squares fits of the Arrhenius plots shown in Fig. 15. E_a has been calculated with the help of Eq. (7). The value of E_a is 80.1, 26.2, and 21.8 kJ/mol for 8CB, 8CB+NFMWCNTs, and 8CB+FMWCNTs, respectively, in the Sm*A* phase whereas the value of E_a is 86.9, 23.4, and 20.6 kJ/mol for 8CB, 8CB+NFMWCNTs, and 8CB+FMWCNTs, respectively, in the *N* phase. The value of E_a is decreased in the dispersed system, which facilitates the easy path for the conduction process by which the σ of both the dispersed systems has increased as compared to the pure sample.

E. Electro-optical studies

Due to the reorientation of directors with applied external perturbation, the electro-optical phenomenon appears in LC molecules [62–64]. When we apply the field to the planar, i.e., homogeneous (HG), aligned molecules in traditional positive dielectric anisotropic materials, the LC molecules attempt to orient in homeotropic (HT) configuration. The Freedericksz transition is a transition from a bright state to a dark state that occurs at a specific voltage. The transmission-voltage curve is shown in Fig. 16. The threshold voltage (V_{th}) is expressed as

$$V_{\text{th}} = \sqrt{\frac{\pi^2 K_{11}}{\varepsilon_0 \Delta\varepsilon'}}, \tag{8}$$

TABLE III. Dielectric and electro-optical parameters for 8CB, 8CB+NFMWCNTs, and 8CB+FMWCNTs.

Material	$\varepsilon'_{\|\|}$	$\varepsilon'_{\perp}$	ε'	$\Delta\varepsilon'$	$\Delta\varepsilon'/\varepsilon'_{\perp}$	V_{th} (V)	K_{11} (pN)	γ (mPa s)
Nematic (34.0 °C)								
8CB	13.7	6.6	8.9	7.1	1.1	0.98	5.7	1.8
8CB+NFMWCNTs	15.2	6.2	9.2	9.0	1.4	0.93	6.9	2.2
8CB+FMWCNTs	16.5	5.5	9.2	11.0	2.0	0.66	4.3	0.9
Smectic (24.0 °C)								
8CB	13.9	6.2	8.8	7.7	1.2	–	–	–
8CB+NFMWCNTs	15.5	5.4	8.8	10.1	1.9	–	–	–
8CB+FMWCNTs	17.5	5.0	9.2	12.5	2.5	–	–	–

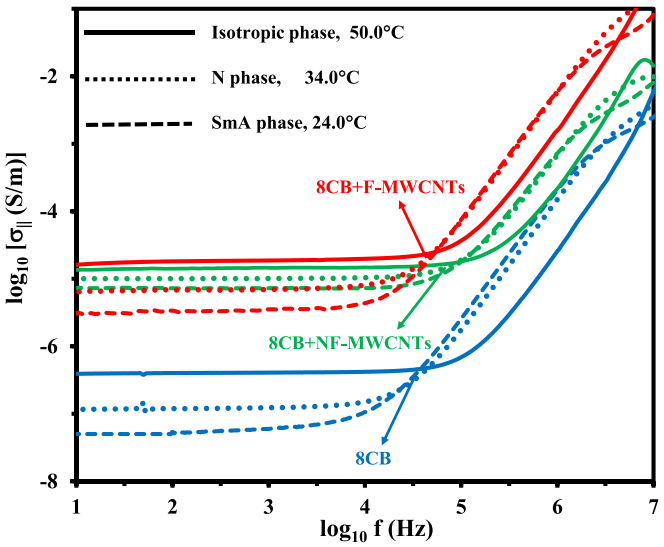

FIG. 14. Frequency dependence of the longitudinal component of the total conductivity in the isotropic, *N*, and Sm*A* phases for pure 8CB and dispersed nanocomposites for homeotropic aligned molecules.

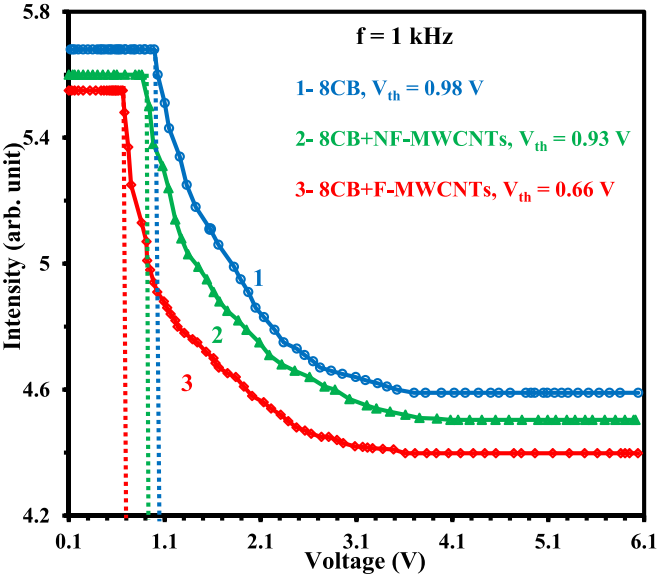

FIG. 16. Transmission voltage (*T-V*) curves for pure and dispersed samples at the frequency of 1 kHz. Curves 1–3 are for pure 8CB, 8CB+NFMWCNTs, and 8CB+FMWCNTs, respectively. Broken vertical lines represent the threshold voltages.

where K_{11} is the splay elastic constant of the material. The value of the V_{th} has been calculated in the *N* (34.0 °C) phase. The value of V_{th} is 0.98, 0.93, and 0.66 V for pure 8CB, 8CB+NFMWCNTs, and 8CB+FMWCNTs, respectively. At lower concentration value V_{th} is 0.88 and 0.79 V for NFMWCNTs and FMWCNTs dispersed nanocomposites [45]. As the concentration is increased the value of V_{th} is increased for NFMWCNTs dispersed nanocomposite while it is decreased for FMWCNTs dispersed nanocomposite. FMWCNTs has a positive impact on the display parameters. A functional group increases the system's dipole moment and polarizability to lower the V_{th} value. Lee and Shih have shown how V_{th} has been reduced by the dispersion of CNTs [65]. MWCNTs work as trapping ions agents where the ions are adsorbed by the surface of tubes [66,67]. The huge surface area, which is where most of the ions are trapped, is related to the high aspect ratio. The reorientation of the LC molecules is lessened if the impurity ions predominate. The diffusion coefficient is also decreased by the insertion of tubes. Along with trapping the ions, CNTs also prevent the ions from moving freely. By adsorbing ions, CNTs also reduce the screening effect in LCs [68–70]. The value of K_{11} is calculated in the *N* (34.0 °C) phase with the help of Eq. (8) and its value is 5.7 pN for pure 8CB, 6.9 pN for 8CB+NFMWCNTs, and 4.3 pN for 8CB+FMWCNTs. The value of K_{11} is decreased for FMWCNTs dispersed nanocomposite while it is increased for NFMWCNTs dispersed nanocomposite. A low value of V_{th} is responsible for the low value of K_{11}. The system's elastic constant has decreased with the addition of a functional group over MWCNTs. Low V_{th} and low K_{11} may be applicable for display material as well as electro-optical devices for FMWCNTs dispersed nanocomposite.

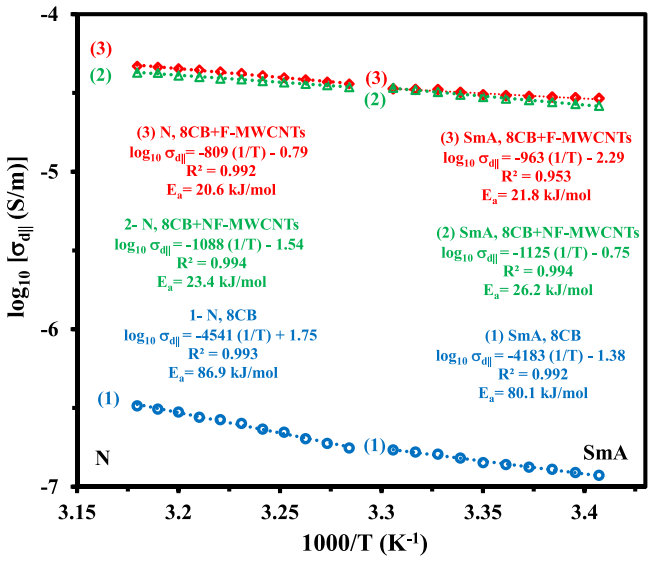

FIG. 15. Variations of longitudinal component of dc conductivity ($\sigma_{d||}$) with the inverse of the absolute temperature (K^{-1}) for (1) 8CB, (2) 8CB+NFMWCNTs,and (3) 8CB+FMWCNTs in the Sm*A* and *N* phases, respectively.

In electro-optical devices, rotational viscosity (γ) is an important parameter and has been measured by different techniques reported in the literature [71,72]. The calculation of γ has been done from the given formula as

$$\gamma = \frac{\tau' K_{11}}{d^2}\pi^2, \tag{9}$$

where τ' represents the relaxation time in the electro-optical measurement. The value of γ is calculated with the help of Eq. (9) in the *N* (34.0 °C) phase. The value of γ is 1.8, 2.2, and 0.9 mPa s for 8CB, 8CB+NFMWCNTs, and 8CB+FMWCNTs, respectively. The attachment of the functional group on the tubes easily rotates the liquid crystalline

molecule in their direction, which is responsible for the low γ of the system. A lower value of K_{11} for FMWCNTs dispersed nanocomposite is also responsible for the lower value of γ. From the electro-optical study, we established that the display parameters have been enhanced by the dispersion of FMWCNTs. Various electro-optical parameters are shown in Table II.

IV. CONCLUSION

We have covered the general aspects of the alignment and interaction of NFMWCNTs and FMWCNTs with LC materials. The thermodynamic investigation shows that the transition temperature is lowered in both nanocomposite systems as compared to the pure 8CB. Due to the establishment of weak hydrogen bonds, the FMWCNT dispersed nanocomposite exhibits a major magnitude of transition temperature lowering. Due to the high dipole moment and polarizability of the nanocomposite system, dielectric investigation demonstrates the increase in the dielectric anisotropy of both dispersed nanocomposites. For the FMWCNTs dispersed nanocomposite, electro-optical experiments demonstrate a decrease in threshold voltage, splay elastic constant, and rotational viscosity. As a result of functional groups being attached to MWCNTs, which makes it easier for molecules to rotate, more liquid crystal ions are adsorbed at the surface of the tubes. The threshold voltage value for the NFMWCNTs dispersed nanocomposite is slightly reduced; however, the splay elastic constant and rotational viscosity are increased. This study also shows that the surface anchoring created by the liquid crystal-FMWCNTs nanocomposite may be advantageous for electro-optical applications. Functionalization has enhanced the tubes' dispersibility, which has a favorable effect on the order parameters and raises the value of permittivity. The electro-optical properties of the liquid crystal-FMWCNTs nanocomposite have also improved because of the easy ion trapping. Thus functionalization of MWCNTs has been advantageous to improve the characteristic parameters of nanocomposites from the application point of view.

ACKNOWLEDGMENTS

We appreciate the financial assistance provided to the Centre of Material Sciences by Department of Science and Technology, New Delhi, through the FIST initiative Grant No. SR/FST/PSI-216/2016. One of us (P.K.S.) expresses thanks to the University Grants Commission, New Delhi, for support through a University Research Fellowship. We thank Dr. Prashant Dubey for producing the functionalized MWCNTs.

P.K.S. performed the conceptualization, investigation, data curation, and writing (original draft preparation). R. Dhar performed the supervision, and reviewing and editing. R. Dabrowski performed the synthesis of the LC material.

No potential conflict of interest was reported by the author(s).

[1] S. Park, M. Vosguerichian, and Z. Bao, Nanoscale **5**, 1727 (2013).
[2] K. Ryu, H. Xue, and J. Park, J. Chem. Technol. Biotechnol. **88**, 788 (2013).
[3] S. Gupta, C. N. Murthy, and C. R. Prabha, Int. J. Biol. Macromol. **108**, 687 (2018).
[4] S. K. Vashist, D. Zheng, K. A. Rubeaan, J. H. T. Luong, and F. S. Sheu, Biotechnol. Adv. **29**, 169 (2011).
[5] M. Bottini, N. Rosato, and N. Bottini, Biomacromolecules **12**, 3381 (2011).
[6] O. Yaroshchuk, S. Tomylko, O. Kovalchuk, and N. Lebovka, Carbon **68**, 389 (2014).
[7] I. Dierking, G. Scalia, P. Morales, and D. LeClere, Adv. Mater. **16**, 865 (2004).
[8] J. P. F. Lagerwall and G. Scalia, J. Mater. Chem. **18**, 2890 (2008).
[9] S. P. Yadav and S. Singh, Prog. Mater. Sci. **80**, 38 (2016).
[10] D. Andrienko, J. Mol. Liq. **267**, 520 (2018).
[11] R. Dhar, Phase Transitions **79**, 175 (2006).
[12] I. Dierking, Liq. Cryst. Today **21**, 47 (2012).
[13] P. Kirsch, and M. Bremer, Angew. Chem., Int. Ed. **39**, 4216 (2000).
[14] S. L. Srivastava and R. Dhar, Indian J. Pure Appl. Phys. **37**, 891 (1999).
[15] W. Lee, C. Y. Wang, and Y. C. Shih, Appl. Phys. Lett. **85**, 513 (2004).
[16] W. Tie, G. H. Yang, S. S. Bhattacharyya, Y. H. Lee, and S. H. Lee, J. Phys. Chem. C **115**, 21652 (2011).
[17] Z. Seidalilir, E. Soheyli, M. Sabaeian, and R. Sahraei, J. Mol. Liq. **320**, 114373 (2020).
[18] J. P. F. Lagerwall and G. Scalia, Curr. Appl. Phys. **12**, 1387 (2012).
[19] J. Prakash, S. Khan, S. Chauhan, and A. M. Biradar, J. Mol. Liq. **297**, 112052 (2020).
[20] M. J. Cho, H. G. Park, H. C. Jeong, J. W. Lee, Y. H. Jung, D. H. Kim, J. H. Kim, J. W. Lee, and D. S. Seo, Liq. Cryst. **41**, 761 (2014).
[21] G. Zhang, X. Chen, J. Zhao, Y. Chai, W. Jhuang, and L. Wang, Mater. Lett. **60**, 2889 (2006).
[22] A. Choudhary, G. Singh, and A. M. Biradar, Nanoscale **6**, 7743 (2014).
[23] S. K. Prasad, M. V. Kumar, T. Shilpa, and C. V. Yelamaggad, RSC Adv. **4**, 4453 (2014).
[24] R. Mishra, J. Hazarika, A. Hazarika, B. Gogoi, R. Dubey, D. Bhattacharjee, K. N. Singh, and P. R. Alapati, Liq. Cryst. **45**, 1661 (2018).
[25] V. Gdovinová, N. Tomašovičová, S. C. Jeng, K. Zakutanská, P. Kula, and P. Kopčanský, J. Mol. Liq. **282**, 286 (2019).
[26] A. Bubnov, A. Bobrovsky, I. Rychetský, L. Fekete, and V. Hamplová, Nanomaterials **10**, 1498 (2020).
[27] A. L. Rodarte, F. Cisneros, J. E. Hein, S. Ghosh, and L. S. Hirst, Photonics **2**, 855 (2015).
[28] B. P. Singh, C. Y. Huang, D. P. Singh, P. Palani, B. Duponchel, M. Sah, R. Manohar, and K. K. Pandey, J. Mol. Liq. **325**, 115130 (2021).

[29] I. Tlili, T. A. Alkanhal, A. A. Barzinjy, R. N. Dara, A. Shafee, and Z. Li, J. Mol. Liq. **294**, 111564 (2019).
[30] R. K. Shukla, A. Chaudhary, A. Bubnov, and K. K. Raina, Liq, Cryst. **45**, 1672 (2018).
[31] K. Scida, P. W. Stege, G. G. Haby, G. A. Messina, and C. D. Garcia, Anal. Chim. Acta **691**, 6 (2011).
[32] K. J. Lee, H. G. Park, H. C. Jeong, D. H. Kim, D. S. Seo, J. W. Lee, and B. M. Moon, Liq. Cryst. **41**, 25 (2014).
[33] R. K. Shukla, A. Chaudhary, A. Bubnov, V. Hamplova, and K. K. Raina, Liq. Cryst. **47**, 1379 (2020).
[34] G. V. Varshini, D. S. S. Rao, P. K. Mukherjee, and S. K. Prasad, J. Mol. Liq. **286**, 110858 (2019).
[35] Neeraj and K. K. Raina, Phys. B: Condens. **434**, 1 (2014).
[36] G. Yadav, K. Agrahari, and R. Manohar, J. Dispersion Sci. Technol. **42**, 707 (2019).
[37] S. K. Supreet, K. K. Raina, and R. Pratibha, Liq. Cryst. **40**, 228 (2013).
[38] Y. P. Sun, K. Fu, Y. I. Lin, and W. Huang, Acc. Chem. Res. **35**, 1096 (2002).
[39] R. Cao, S. Chen, Y. Wang, N. Han, H. Liu, and X. Jhang, Carbon **149**, 263 (2019).
[40] N. Dalir and S. Javadian, J. Mol. Liq. **341**, 117287 (2021).
[41] M. C. Cetinkaya, S. Yildiz, and H. Ozbek, J. Mol. Liq. **272**, 801 (2018).
[42] J. Kumar, V. Manjuladevi, R. K. Gupta, and S. Kumar, Liq. Cryst. **42**, 361 (2015).
[43] M. Mishra, R. S. Dabrowski, J. K. Vij, A. Mishra, and R. Dhar, Liq. Cryst. **42**, 1580 (2015).
[44] S. Sridevi, S. K. Prasad, G. G. Nair, V. D. Britto, and B. L. V. Prasad, Appl. Phys. Lett. **97**, 151913 (2010).
[45] P. K. Singh, P. Dubey, R. Dhar, and R. Dabrowski, J. Mol. Liq. **369**, 120889 (2023).
[46] *User's Manual*, Netzsch DSC model-DSC-200-F3-Maia, Netzsch Gerätebau GmbH, Selb, Germany.
[47] N. Yadav, R. Dabrowski, and R. Dhar, Liq. Cryst. **41**, 1803 (2014).
[48] M. Mishra, R. S. Dabrowski, and R. Dhar, J. Mol. Liq. **213**, 247 (2016).
[49] T. L. A. Montanheiro, F. H. Cristóvan, J. P. B. Machado, D. B. Tada, N. Duran, and A. P. Lemes, J. Mater. Res. **30**, 55 (2015).
[50] M. V. Gorkunov and M. A. Osipov, Soft Matter **7**, 4348 (2011).
[51] V. Popa-Nita and S. Kralj, J. Chem. Phys. **132**, 024902 (2010).
[52] X. Chen, W. Xiaoli, Z. Jiagui, L. Jilin, and C. Jianghua, Mater. Sci. Eng. B **176**, 425 (2011).
[53] P. K. Singh, P. Dubey, R. Dabrowski, and R. Dhar, Liq. Cryst. **49**, 456 (2022).
[54] R. Dhar, Indian J. Pure Appl. Phys. **42**, 56 (2004).
[55] K. S. Cole and R. H. Cole, J. Chem. Phys. **9**, 341 (1941).
[56] S. L. Srivastava and R. Dhar, Indian J. Pure Appl. Phys. **29**, 745 (1991).
[57] R. Dhar, J. Mol. Liq. **343**, 117682 (2021).
[58] R. K. Shukla, K. K. Raina, V. Hamplová, M. Kašpar, and A. Bubnov, Phase Transitions **84**, 850 (2011).
[59] R. Dabrowski, Liq. Cryst. **42**, 344 (2015).
[60] A. K. Jonscher, J. Mol. Liq. **86**, 259 (2000).
[61] S. L. Srivastava and R. Dhar, Radiat. Phys. Chem. **47**, 287 (1996).
[62] S. Yildiz, I. Koseoglu and M. C. Cetinkaya, J. Mol. Liq. **209**, 729 (2015).
[63] L. A. Dolgov, N. I. Lebovka, and O. V. Yaroshchuk, Colloid J. **71**, 603 (2009).
[64] C. Y. Huang, H. C. Pan, and C. T. Hsieh, Jpn. J. Appl. Phys. **45**, 6392 (2006).
[65] C. W. Lee and W. P. Shih, Mater. Lett. **64**, 466 (2010).
[66] I. S. Baik, S. Y. Jeon, S. H. Lee, K. A. Park, S. H. Jeong, K. H. An, and Y. H. Lee, Appl. Phys. Lett. **87**, 263110 (2005).
[67] A. G. García, R. Vergaz, J. F. Algorri, X. Quintana, and J. M. Oton, Beilstein J. Nanotechnol. **6**, 396 (2015).
[68] S. Schymura and G. Scalia, Philos. Trans. R. Soc. A **371**, 20120261 (2013).
[69] Y. J. Lima, S. S. Bhattacharyya, W. Tie, H. R. Parka, Y. H. Lee, and S. H. Lee, Liq. Cryst. **40**, 1202 (2013).
[70] M. D. Lynch and D. L. Patrick, Nano Lett. **2**, 1197 (2002).
[71] A. Chakraborty, M. K. Das, B. Das, U. Baumeister, and W. Weissflog, J. Mater. Chem. C. **1**, 7418 (2013).
[72] P. Sathyanarayana, B. K. Sadashiva, and S. Dhara, Soft Matter **7**, 8556 (2011).